Design and Analysis of Stacked Micromirrors

Sangtak Park[*,1], So-Ra Chung[2], and John T.W. Yeow[3]
[1,2,3] University of Waterloo, Systems Design Engineering
[*]Systems Design, University of Waterloo, 200 University Ave. West, Waterloo, Ontario, N2L 3G1, Canada

Abstract: A micromirror or a torsional actuator in general has been proven to be one of the most popular actuators fabricated by Micro-Electro-Mechanical System (MEMS) technology in many industrial and biomedical applications such as RF switches, a laser scanning display, an optical switch matrix, and biomedical image systems. Even though there are many different actuation mechanisms for a micromirror, the electrostatic actuation has been most popular due to its well-studied nature and simple configuration. However, the actuation voltage can be quite high and the angular deflection might be too small. In this paper, two stacked micromirrors are presented and analyzed to show better performance than that of the conventional micromirror in terms of angular deflection and actuation voltage. The pull-in voltage of two stacked micromirrors is also derived analytically and compared with that of the conventional micromirror. FEM is created in COMSOL to verify the stacked micromirrors' analytical result.

Keywords: MEMS, Stacked Micromirror, Moving Electrodes, Electrostatic Actuation, Pull-In Voltage

1. Introduction

Development of Micro-Electro-Mechanical Systems (MEMS) technology in the past decades has benefited automotive, communication and medical industries where size and mass reduction improved the performance of the devices such as accelerometers for inertial measurement, mass-flow sensors, and bio-chips for microfluidics, RF switches and automotive pressure sensors [1]. Popular MEMS devices in the optical application are optical switch arrays for communication, Optical Coherence Tomography (OCT) for an endoscope [3], a Confocal Laser Scanning Microscopy (CLSM) for obtaining high resolution images, and the digital micromirror device for Digital Light Process (DLP) Projection from Texas Instrument. The micromirrors in above devices can be actuated by electrostatic, electromagnetic, electrothermal or piezoelectric mechanisms.

Despite the pull-in effect, nonlinear behavior, and high operating voltage, the electrostatic actuation is one of preferred choices for micromirror actuation due to advantages of the low power consumption, fast response time, and the easiness of integration and fabrication. The actuation voltage of the micromirror can be lowered while achieving more deflection if the stiffness of torsion bars is reduced. However, when the stiffness is reduced the natural frequency of the micromirror also decreases, thereby limiting operational frequency. In this paper, two novel configurations of stacked micromirrors are presented. The proposed configurations have the potential to achieve more deflection at lower actuation voltage without sacrificing high frequency performance.

The proposed design and the analytical model of the micromirror in stacked configurations are presented and derived in the section 2. The geometry of stacked micromirrors is described in detail and the finite element analysis results in COMSOL are discussed in the section 3. The final section provides the conclusion of the findings.

2. Analytical Model of the Stacked Mirror

In this section, the micromirror in different stacked configurations is presented and its analytical model is also derived. The conceptual schematics of the three different configurations are shown in the following. The moving electrode in the stacked configurations is assumed to be identical to the micromirror in terms of shape, size and material to simplify the analysis. Furthermore, the fixed bottom electrodes are not considered in this analysis and not actuated.

A conventional micromirror is shown in **Figure 1**. **Figure 2** and **3** show the stacked micromirror without offset and the stacked micromirror with offset, respectively. **D** denotes an initial gap between the micromirror and its electrodes. **L** is equal to a half length of the micromirror.

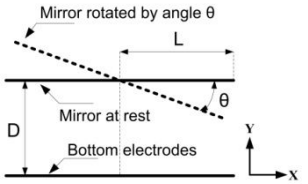

Figure 1. Schematic of Conventional Micromirror

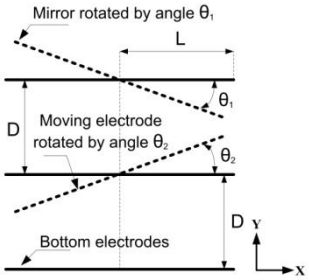

Figure 2. Stacked Micromirror without Offset

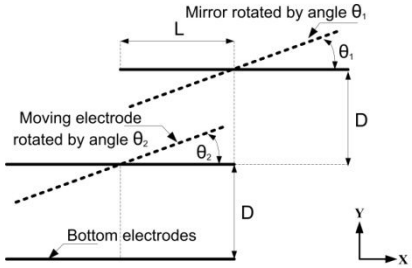

Figure 3. Stacked Micromirror with Offset

First, the dynamic equation of the conventional mirror in **Figure 1** is derived and shown below.

$$\mathrm{I}\frac{d^2\theta}{dt^2} + c\frac{d\theta}{dt} + k\theta = M \qquad (1)$$

where, **I** is the moment of the inertia of the micromirror along the z axis. **c** is the damping coefficient representing the squeeze-film damping. **k** is the torsional stiffness of the rotated serpentine spring. **θ** represents the angular displacement from the rest state. **M** is the torque created by the electrostatic force between the micromirror and its electrodes.

Second, the value for damping coefficient, **c**, representing the squeeze-film damping of the micromirror is derived from the linearized Reynold's equation [4] and presented in Equation (2).

$$c = -\frac{48\mu L w^5}{\pi^6(b^2+4)D^3} \qquad (2)$$

where, **μ** is the dynamic viscosity of the air. **w** is the width of the micromirror. **b** is the ratio of the width to the length of the micromirror.

Third, the torsional stiffness, **k**, of the rotated serpentine spring is derived based on the Equation (3) from work of G. Barillaro *et. Al* [5] and J. You *et. al* [6]

$$k = \frac{GJ_p}{(2N+3)l_p} \qquad (3)$$

where, **G** is the shear modulus of the material used in the rotated serpentine spring. $\mathbf{J_p}$ is the torsion factor of a beam with rectangular cross-section [5] and can be derived from the Equation (4) below. **N** is the number of the loops or turns in the rotated serpentine spring. $\mathbf{l_p}$ is the length of the rotated serpentine spring segment that is parallel to the rotation axis.

$$J_p = \frac{tw^3}{3}\left(1 - \frac{192w}{\pi^5 t}\sum_{i=1,3,5\ldots}\frac{1}{i^5}\tanh\left(\frac{i\pi t}{2w}\right)\right) \qquad (4)$$

Fourth, for the sake of simplicity, the micromirror is considered to be a rigid body and the deflection of the rotated serpentine spring in the y axis is assumed to be negligible. The torque created by the electrostatic force between the micromirror and its electrodes denoted by **M** for each configuration is derived by using the parallel-plate capacitor theorem. The differential force acting on an infinitesimal segment of the micromirror and its electrodes is derived and then the torque is obtained by integrating this force over a half length of the micromirror: [2]

$$dF = \frac{1}{2}\varepsilon V^2\frac{wdx}{(D-x\sin\theta)^2} \qquad (5)$$

$$M = \int_0^L xdF = \frac{\varepsilon w V^2}{2}\int_0^L \frac{x}{(D-x\sin\theta)^2}dx$$
$$= \frac{\varepsilon w V^2}{2\sin^2\theta}\left\{\frac{L\sin\theta}{D-L\sin\theta} + \ln\left(1-\frac{L}{D}\sin\theta\right)\right\} \qquad (6)$$

where, **ε** denotes the permittivity of the air. **V** represents the potential difference between the micromirror and its electrode.

Last, the normalized angle φ and the maximum deflection angle θ_{max} are defined in the following.

$$\varphi = \frac{\sin\theta}{\sin\theta_{max}} \approx \frac{\theta}{\theta_{max}},\ \theta_{max} = \sin^{-1}\frac{D}{L} \approx \frac{D}{L}$$
$$,if\ \theta \ll 1\ and\ \theta_{max} \ll 1 \qquad (7)$$

The calculated torque **M** for each configuration is simplified with the normalized angle φ as the following Equation (8), (9) and (10).

$$M_1 = \frac{1}{2}\varepsilon w V^2 \frac{L^2}{D^2}\frac{1}{\varphi^2}\left(\frac{\varphi}{1-\varphi} + \ln(1-\varphi)\right) \quad (8)$$

$$M_2 = \frac{1}{2}\varepsilon w V^2 \frac{L^2}{D^2}\frac{1}{4\varphi^2}\left(\frac{2\varphi}{1-2\varphi} + \ln(1-2\varphi)\right) \quad (9)$$

$$M_3 = \frac{1}{2}\varepsilon w V^2 \frac{L^2}{D^2}\frac{1}{2}\left(\frac{1}{1-2\varphi+\varphi^2}\right) \quad (10)$$

where, $\mathbf{M_1}$ represents the torque acting on the conventional micromirror in **Figure 1**. $\mathbf{M_2}$ and $\mathbf{M_3}$ denote the torque generated in the stacked micromirror without offset shown in **Figure 2** and in the stacked micromirror with offset shown in **Figure 3**, respectively. To simplify the analysis, the bottom electrodes are not used to actuate the micromirrors in both stacked configurations.

To visualize the difference in the magnitude of the generated torque of three configurations, the normalized torque and angular displacement are shown in **Figure 4**. As expected, there is not much discernable difference in the region of small angular displacement. However, while the angular displacement of the conventional mirror increases almost linearly, the stacked mirror without offset experiences exponential growth in its angular displacement.

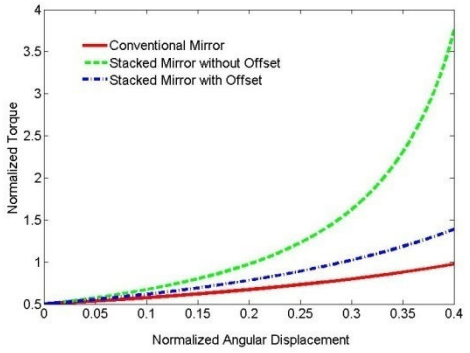

Figure 4. Normalized Angular Displacement and Normalized Torque

However, there is no information in **Figure 4**, regarding when the pull-in occurs. When the open loop voltage-control method is used to actuate the micromirrors, the pull-in is inevitable. Hence, it is important to obtain the information on the pull-in. To emphasize the difference in the pull-in voltage and the angular displacement of three configurations, the angular deflection is plotted against the normalized actuation voltage in **Figure 5**. Even though the staked mirror without offset is displaced more at the same actuation voltage, it also experiences the pull-in at the lower voltage. The pull-in voltage and angular deflection of the micromirror can be derived from the analytical model using the total potential energy of the system denoted by **U**.

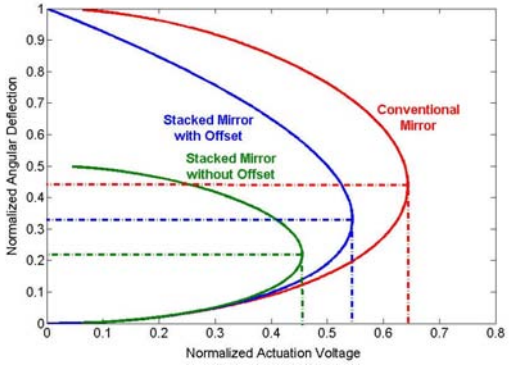

Figure 5. Normalized Actuation Voltage vs Normalized Angular Displacement

$$U = U_{me} + U_{es} \quad (11)$$

$$U = 2 \times \frac{1}{2}k\theta^2 - \frac{\varepsilon w V^2}{2}\int_0^L \frac{dx}{(D - x\sin\theta)} \quad (12)$$

where, $\mathbf{U_{me}}$ represents the strain energy stored in two torsional springs. $\mathbf{U_{es}}$ denotes the electrostatic energy stored between the micromirror and its electrodes. Applying the small angle approximation, this equation can be expressed in terms of the normalized angle φ.

$$U = k\frac{D^2}{L^2}\varphi^2 + \frac{\varepsilon w V^2}{2}\frac{L}{D}\frac{1}{\varphi}\ln(1-\varphi) \quad (13)$$

Since the pull-in is an unstable fixed point, it can be found by solving the second derivative of **U** in terms of the normalized angle φ.

$$\left.\frac{\partial^2 U}{\partial \varphi^2}\right|_{pull-in} = 0 \quad (14)$$

By solving Equation (14), the normalized angle at the pull-in is obtained and is shown below.

Moreover, if the pull-in angle is known, the pull-in voltage can also be calculated using the relationship between the electrostatic torque and the stiffness of the torsional springs.

$$\varphi_{1,pull-in} = 0.4404$$

$$V_{1,pull-in} = \sqrt{1.655\frac{kD^3}{\varepsilon wL^3}} \quad (15)$$

The same steps can be followed to find out the angle at the pull-in and the pull-in voltage of the stacked micromirrors. The total potential energy of the stacked micromirror without offset is derived in Equation (16) and then, it is expressed in terms of the normalized angle in Equation (17).

$$U = 4 \times \frac{1}{2}k\theta^2 - \frac{\varepsilon wV^2}{2}\int_0^L \frac{dx}{(D-2xsin\theta)} \quad (16)$$

$$U = 2k\frac{D^2}{L^2}\varphi^2 + \frac{\varepsilon wV^2}{4}\frac{L}{D}\frac{1}{\varphi}\ln(1-2\varphi) \quad (17)$$

$$\varphi_{2,pull-in} = 0.2202$$

$$V_{2,pull-in} = \sqrt{0.8274\frac{kD^3}{\varepsilon wL^3}} \quad (18)$$

For the stacked micromirror with offset, the same steps are followed to obtain the pull-in angle and the pull-in voltage.

$$U = 4 \times \frac{1}{2}k\theta^2 - \frac{\varepsilon wV^2}{2}\int_0^L \frac{dx}{(D-Lsin\theta)} \quad (19)$$

$$U = 2k\frac{D^2}{L^2}\varphi^2 - \frac{\varepsilon wV^2}{2}\frac{L}{D}\frac{1}{(1-\varphi)} \quad (20)$$

$$\varphi_{3,pull-in} = 0.33\dot{3}$$

$$V_{3,pull-in} = \sqrt{1.185\frac{kD^3}{\varepsilon wL^3}} \quad (21)$$

3. Finite Element Analysis in COMSOL

The size and geometry of the micromirror are determined by an optical beam size as well as the application. For example, the micromirror implemented in an endoscope would require a small form factor, for it operates inside of human cavity. At the same time, it should be big enough to fully accommodate a size of an optical beam. In this analysis, the micromirror is decided to be 1 mm in length, 1mm in width and 10 μm in thickness, as shown in **Figure 6**-b. It is also assumed to be made of polysilicon with Young's modulus of 160 GPa, Poisson's ratio of 0.22 and 2330 kg/m^3 in density. The micromirror is suspended over a cavity by two torsion bars. Even though a straight torsion bar is simple to design and fabricate, it suffers from a residual stress, which alters the stiffness of a torsion bar and the frequency response of the micromirror. Furthermore, physical and geometric properties of a straight torsion bar cannot be easily adjusted or modified, because the geometry of a torsion bar such as width and thickness is limited by the fabrication process. Thus, two rotated serpentine springs are chosen to hold the micromirror in place for design flexibility, because the serpentine springs' stiffness can be easily customized regardless of fabrication process. The rotated serpentine spring is well analyzed in [5] and has been fabricated [6]. Thus the rotated serpentine spring is employed in this analysis. The rotated serpentine spring used in this analysis is 4 μm wide, 10 μm thick, and 100 μm in length from one end to another end. The gap between each turn is also 4 μm and it is made of the same polysilicon as the micromirror. **Figure 6** shows the zoomed-in view of the rotated serpentine spring, and the relative size and location of the spring on the micromirror.

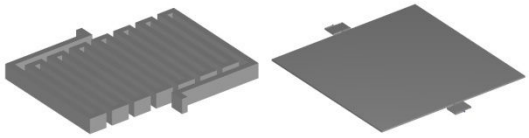

(a) (b)

Figure 6. Rotated Serpentine Spring (a) and Micromirror (b)

To simplify the modeling and analysis, the geometry and material of the micromirror are kept identical except for the stacking method. As shown in **Figure 7**-a, the micromirror is placed 250 μm right above the moving electrode along the y axis, creating the stacked micromirror without offset. In **Figure 7**-b, the micromirror is put above the moving electrode with 250 μm gap in the y axis as well as 500 μm offset in the x axis. The micromirror and its moving electrodes have two electrodes located on their bottom and the electrodes are assumed to be aluminum

deposited on the polysilicon in 1 μm thick. The rotated serpentine springs provide electrical connection between the electrodes and control circuitry.

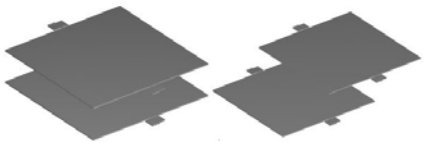

(a) (b)

Figure 7. Stacked Mirror without Offset (a) and Stacked Mirror with Offset (b)

Three finite element models are created to represent each micromirror configuration discussed in the analytical section: (i) a single mirror with fixed bottom electrodes shown in **Figure 8**-a; (ii) a stacked mirror without an offset in **Figure 8**-b; and (iii) a stacked mirror with an offset shown in **Figure 8**-c.

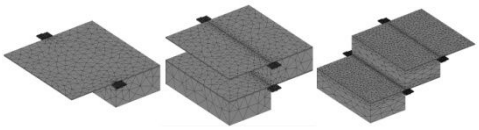

(a) (b) (c)

Figure 8. FEMs of Three Micromirror Configurations

For the static analysis, the actuation voltage is increased gradually to find the angular deflection of the micromirror. Both stacked micromirrors show more deflection than that of the conventional micromirror as the actuation voltage increases. As mentioned before, there is not much difference in deflection at low actuation voltage, because the initial gap is the same along the edge of the micromirror. However, the difference in angular deflection becomes clear at higher actuation voltage until the pull-in occurs. Furthermore, the micromirror in the stacked configuration without offset shows more deflection than the stacked micromirror with offset. The reason is that more charges are concentrated and induced at the far edge of the micromirror, where the gap between the micromirror and its electrodes is smallest. Thus, the surface charge density is the highest in the far edge, creating the most torque. On the contrary, the charges are uniformly distributed in the stacked micromirror with the offset, resulting in less torque, since the air gap along the surface is rather uniform while rotating. This simulation result is shown in **Figure 9**.

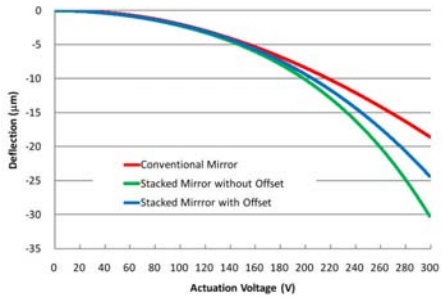

Figure 9. Static Analysis Results of Three Micromirror Configurations

The two stacked micromirrors post-processed with their displacement in the y axis are shown in **Figure 10**. As expected, the magnitude of deflection in the micromirror is equal to that of the moving electrodes in an opposite direction.

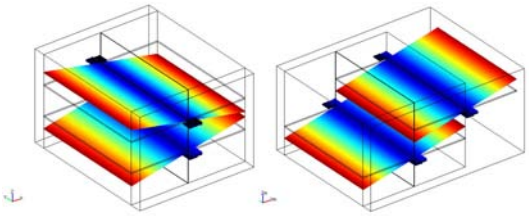

(a) (b)

Figure 10. Micromirrors Post-processed with Deflection

In order to achieve more deflection at even lower actuation voltage, the fixed bottom electrodes on top of the substrate can be activated. Even though there is no analytical model predicting the deflection of the micromirror, more deflection would be expected intuitively. **Figure 11** shows the micromirrors deflected with activated bottom electrodes.

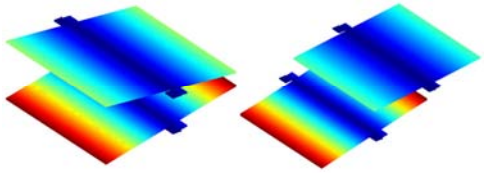

(a) (b)

Figure 11. Deflected Micromirrors with Activated Bottom Electrodes

The eigenfrequency analysis is also performed to obtain the natural frequency of the micromirror. Its first natural frequency is 543 Hz, rotating about the z axis shown in **Figure 12**-a and the

second natural frequency is 3602 Hz, rectilinear motion in the z axis shown in **Figure 12**-b, and the third natural frequency is 3910 Hz, rectilinear motion along the y axis.

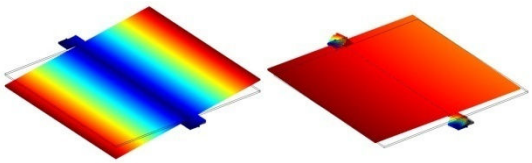

(a) (b)

Figure 12. Normal Mode Analysis

For a scanning micromirror, its transient performance is more important than the static performance. Most scanning micromirrors operate in their resonant mode, at the frequency close to their natural frequency in order to achieve a bigger angular deflection at the lower actuation voltage. Both frequency responses with and without damping are shown in Figure 9. In the damped frequency response analysis, only the squeeze-film damping is considered and any structural damping is not included. It turns out that the squeeze-film damping is negligible with 250 μm gap.

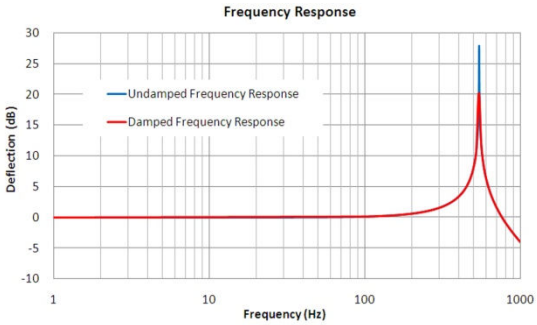

Figure 13. Frequency Response of Micromirror

4. Conclusions

The micromirror in two different stacked configurations is studied and numerically analyzed in this paper. Its analytical model is also derived to facilitate comparisons of its performance against a conventional micromirror. Then, its FEM is created and simulated in COMSOL to show better static and transient performance over the others. Even though the moving electrode in this design is assumed to be identical to the micromirror in terms of its size and torsional stiffness, changes to the electrode can be made to meet specific application requirements. Furthermore, this concept can be easily extended to a 2 DOF micromirror.

5. References

1. Stephen D. Sentruria, “Microsystem Design”, *Kluwer Academic Publishers*, (2001)

2. R. Sattler, F. Plotz, G. Fattinger, G.Wachutka, “Modeling of an electrostatic torsinal actuator: demonstrated with an RF MEMS switch”, *Sensors and Actuators A:Physical*, 337-346 (2002)

3. J. T. W. Yeow, V. X. D. Yang, A. Chahwan, M. L. Gordon, B. Qi, I. A. Vitkin, B. C. Wilson, A. A. Goldenberg, "Micromachined 2-D scanner for 3-D optical coherence tomography", *Sensors and Actuators A:Physical*, 331-340 (2005)

4. Feixia Pan, Joel Kubby, Eric Peeters, Alex T. Tran, Subrata Mukherjee, "Squeeze Film Damping Effect on the Dynamic Response of a MEMS Torsion Mirror", *International Conference on Modeling and Simulation of Microsystems*, 474-479 (1998)

5. Giuseppe Barillaro, Antonio Molfese, Andrea Nannini and Francesco Pieri, "Analysis, Simulation and relative performances of two kinds of serpentine springs", *Journal of Micromechnics and microengineering*, 736-746 (2005)

6. Jianliang You, Muthukumaran Packirisamy, Ion Stiharu, "Analysis, Simulation and Testing of a Micromirror with Rotational Serpentine Springs", *Intelligent Sensing and Information Processing*, 219-225 (2005)